Advances in Nano Research, *Vol. 8 No. 1 (2020) 83-94*
DOI: https://doi.org/10.12989/anr.2020.8.1.083

Thermal buckling analysis of magneto-electro-elastic porous FG beam in thermal environment

Farzad Ebrahimi*[1], Ali Jafari[1] and Rajendran Selvamani[2]

[1] *Department of Mechanical Engineering, Faculty of Engineering, Imam Khomeini International University, Qazvin, Iran*
[2] *Department of mathematics, Karunya Institute of Technology and Sciences, Coimbatore, India*

(*Received April 25, 2019, Revised September 27, 2019, Accepted October 27, 2019*)

Abstract. An analytical formulation and solution process for the buckling analysis of porous magneto-electro-elastic functionally graded (MEE-FG) beam via different thermal loadings and various boundary conditions is suggested in this paper. Magneto electro mechanical coupling properties of FGM beam are taken to vary via the thickness direction of beam. The rule of power-law is changed to consider inclusion of porosity according to even and uneven distribution. Pores possibly occur inside FGMs due the result of technical problems that lead to creation of micro-voids in these materials. Change in pores along the thickness direction stimulates the mechanical and physical properties. Four-variable tangential-exponential refined theory is employed to derive the governing equations and boundary conditions of porous FGM beam under magneto-electrical field via Hamilton's principle. An analytical model procedure is adopted to achieve the non-dimensional buckling load of porous FG beam exposed to magneto-electrical field with various boundary conditions. In order to evaluate the influence of thermal loadings, material graduation exponent, coefficient of porosity, porosity distribution, magnetic potential, electric voltage and boundary conditions on the critical buckling temperature of the beam made of magneto electro elastic FG materials with porosities a parametric study is presented. It is concluded that these parameters play remarkable roles on the buckling behavior of porous MEE-FG beam. The results for simpler states are proved for exactness with known data in the literature. The proposed numerical results can serve as benchmarks for future analyses of MEE-FG beam with porosity phases.

Keywords: buckling analysis; magneto-electro-elastic porous FG beam; thermal loading; refined beam theory

1. Introduction

Magneto-electro-elastic materials (MEEMs) as one of the special sorts of smart materials have received much attention in engineering structures during the recent years. The two-phase composites of piezoelectric and piezo-magnetic materials which is a strong magneto-electrical coupling effect was discovered in 1990s, which has potential practical application in many fields and reported that this coupling effect cannot be found in a single-phase material. Furthermore, MEE materials shows some fascinating properties such as the piezo-electric, piezo-magnetic and magneto-electric significance in which the elastic deformations may be produced directly by mechanical loading or indirectly by an application of electric or magnetic field. The mechanical behaviors of magneto-electro-elastic structures have received notable attention by many researchers in the recent years. Among them, analytical solutions for studying magneto-electro-elastic responses of beams is presented by Jiang and Ding (Jiang and Ding 2004). Most recently, based on three-dimensional elasticity theory and employing the state space approach, Xin and Hu (2015) presented semi-analytical evaluation of free vibration of arbitrary layered magneto-electro-elastic beams.

Functionally graded materials (FGMs) as a new class of composite structures have attracted many researchers in the smart materials and structures by minimizing or removing stress concentrations at the interfaces of the traditional composite materials. The material properties of FGMs have continual changes in one or more directions. Recently, FGMs have received wide applications as structural components in modern industries such as mechanical, civil, nuclear reactors, and aerospace engineering. Numerous studies have been conducted for investigation the mechanical responses of FG structures (Lu and Chen 2005, Tahouneh 2014). In the recent years, several researchers examined mechanical properties of structural elements made from magneto-electro-elastic functionally graded (MEE-FG) materials. Kattimani and Ray (2015) verified the large amplitude vibration responses of magneto electro elastic FGM plates. Static behavior of a circular MEE-FG plate is analyzed by Sladek *et al.* (2015) by using a meshless method. Analytical solutions for studying magneto-electro-viscoelastic responses of nanobeams is presented by Ebrahimi and Barati (2016b). In another survey, thermal buckling of embedded MEE-FG nano plate were inspected by Barati *et al.* (2016) based on a new refined trigonometric plate theory. In another research a pin-moment model of flexoelectric actuators was presented by Wang *et al.* (2018) and an electro-hydrostatic actuator for hybrid active-passive vibration isolation by Henderson

*Corresponding author, Ph.D.,
E-mail: febrahimy@eng.ikiu.ac.ir

http://www.techno-press.org/?journal=journal=anr&subpage=5
ISSN: 2287-237X (Print), 2287-2388 (Online)

et al. (2018). Also, active vibration compensator on moving vessel by hydraulic parallel mechanism examined by Tanaka (2018).

The recent developments in technology of structural elements, structures with graded porosity can be introduced as one of the latest development in FGMs. The structures consider pores into microstructures by taking the local density into account. Researches focus on development in preparation methods of FGMs such as powder metallurgy, vapor deposition, self-propagation, centrifugal casting, and magnetic separation (Khor and Gu 2000, Seifried *et al*. 2001, Watanabe *et al*. 2001, Peng *et al*. 2007, Song *et al*. 2007). These methods have their own ineffectiveness such as high costs and complexity of the technique. An efficient way to manufacture FGMs is sintering process in which due to difference in solidification of the material constituents, porosities or micro-voids through material can create (Zhu *et al*. 2001). Researchers investigated the existence of porosities in FGMs fabricated by a multi-step sequential infiltration technique (Wattanasakulpong *et al*. 2012). By keeping the available information about porosities in FGMs in mind, it is necessary to study the porosity impact when designing and analyzing FGM structures. Porous FG structures having the combination of high stiffness in conjunction with very law specific weight which leads an excellent mechanical properties (Rezaei and Saidi 2016). A few investigations on the mechanical responses of porous FG structures are available in literature. Wattanasakulpong and Ungbhakorn (2014) studied the linear and non-linear vibration of porous FGM beams with elastically restrained ends. Moreover, Yahia *et al*. (2015) study the porosity effect on the wave propagation of FG plates by using various higher-order shear deformation theories. Ebrahimi *et al*. (2016) suggested a model for thermo-mechanical vibration response of temperature-dependent porous FG beams subjected to various temperature risings based on Euler Bernoulli beam theory. Further, Ebrahimi and Mokhtari (2015) considered differential transform method for the vibration of rotating porous beam. Moreover, Ebrahimi and Hashemi (2015) have taken double taper effect on the vibration of rotating porous beam. In the other research Ebrahimi and Zia (2015) utilized Galerkinʼs method and the method of multiple scales to present nonlinear vibration behavior of FG Timoshenko beam with porosites. Recently, Mechab *et al*. (2016) developed a nonlocal elasticity model for free vibration of FG porous nanoplates resting on elastic foundations. Boutahar and Benamar (2016) presented a semi analytical method for non-linear vibration analysis of FGM porous annular plates resting on elastic foundations.

Recently, it is well understood from the studies that classic beam theory (CBT) is not appropriate for thick beams and higher modes of vibration due to the lack in impact of shear deformation. Hereupon, first order shear deformation theory (FSDT) is suggested to overcome the defects of CPT with supposition a shear correction factor in the thickness direction of beam. As regards FSDT isn’t able to evaluate the zero-shear stress on the top and bottom surfaces of the beam, there appeared a need to develop higher order theory (HOT). This theory doesn’t need any shear correction factors and predict transverse shear stresses properly. Many published work has been utilized the HOT method to investigate mechanical response of FG structures (Kant and Swaminathan 2000, Yahia *et al*. 2015). Based on HOBT, Kadoli *et al*. (2008) verified the static response of FG beams under environment temperature. Larbi *et al*. (2013) developed an efficient shear deformation beam theory for investigating static and vibrational of FG beam. By developing a novel refined theory, Vo *et al*. (2014)investigated static and vibration behavior of FG beams. In another study, Vo *et al*. (2015) has taken a quasi-3D theory to study vibration and buckling behavior of FG sandwich beams. Atmane *et al*. (2015) used a more efficient beam theory to study the effects of thickness stretching and porosity on mechanical responses of bedded FGM beams resting on elastic foundation. One of the main mechanical characteristics of FG structures is the buckling response which play a notable role on the safety of engineering structures, and accordingly has received intense attention by several researchists (Liew *et al*. 2004, Yang *et al*. 2006, Ke *et al*. 2012, Şimşek and Yurtcu 2013). In addition, as it is obviously known one of the most important features of FG materials is thermal insulations, hence it is essential to assume changing porous material properties due to thermal environment, for example, under a high temperature environment the materials become softer, Young’s modulus and thermal expansion often will be decrease with rising temperature. So, it is necessary to consider changes in material properties (Ebrahimi and Barati 2016b, Ebrahimi and Jafari 2016a, b). Therefore, With the wide application of magneto electro porous FG structures, understanding buckling of MEE-FG porous beam subjected to different thermal loadings becomes an important task.

From the literature reviewed above, it is evident that no paper published in the title of thermo-mechanical buckling of MEE-FG porous beam. According to wide application of magneto electro elastic porous FG structures, understanding buckling behavior of MEE-FG porous beam exposed to different thermal loadings becomes important issue in engineering structures. The aim of this study is to develop an analytical solution for check the buckling behavior of smart FG porous beam under thermal, magnetic and electric field with various boundary conditions via refined beam theory. Three types environmental conditions namely, uniform, linear and sinusoidal temperature rises trough the thickness direction are considered. Two kinds of porosity distribution namely even and uneven through the thickness directions are considered. The modified power-law model is exploited to describe gradual variation of magneto electro mechanical material characteristics of porous MEE-FG beam. Governing equations of higher order MEE-FG beam are obtained together via Hamilton’s equation and four-variable refined shear deformation theory and they are solved applying an analytical solution method. Several numerical exercises are presented investigating the influences of porosity, type of porous distribution, thermal effect, external electric voltage, magnetic potential, material graduation index and boundary condition on the thermos-mechanical buckling behavior of MEE-FG porous beam.

Table 1 Magneto-electro-elastic coefficients of material properties

Properties	$BaTiO_3$	$CoFe_2O_4$	Properties	$BaTiO_3$	$CoFe_2O_4$
$c_{11} = c_{22}$ (GPa)	166	286	e_{15}	11.6	0
c_{33}	162	269.5	q_{31} (N/Am)	0	580.3
$c_{13} = c_{23}$	78	170.5	q_{33}	0	699.7
c_{12}	77	173	q_{15}	0	550
c_{55}	43	45.3	s_{11} $(10^{-9}C^2m^{-2}N^{-1})$	11.2	0.08
c_{66}	44.5	56.5	s_{33}	12.6	0.093
e_{31} (Cm^{-2})	-4.4	0	$\chi_{11}(10^{-6}Ns^2C^{-2}/2)$	5	-590
e_{33}	18.6	0	χ_{33}	10	157
ρ (kgm^{-3})	5800	5300	$d_{11} = d_{22} = d_{33}$	0	0

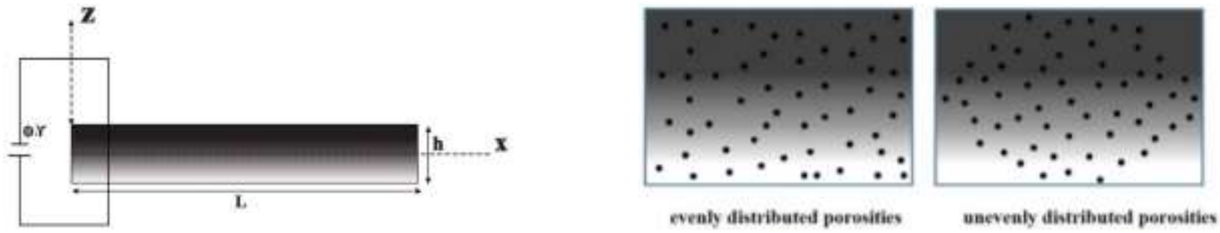

Fig. 1 Geometry and cross section of porous FGM beam under magneto-electrical field

2. Theoretical formulations

2.1 The material properties of porous magneto-electro-elastic FG beam

A magneto-electro-elastic functionally graded beam with two different porosity distribution and rectangular cross-section of width$b$and thickness$h$is taken for this study (Fig. 1). MEE-FG beam is composed of $BaTio_3$ and $CoFe_2O_4$ materials with the material properties presented in Table 1 and exposed to a magnetic potential $\gamma(x,z,t)$ and electric potential $\Phi(x,z,t)$. The effective material properties of MEE-FG beam change continuously in the thickness direction according to modified power-law distribution. The effective material properties (P_f) of porous FGM beam by using the modified rule of mixture can be expressed by Wattanasakulpong and Ungbhakorn (2014)

$$P_f = P_u(V_u - \frac{\alpha}{2}) + P_l(V_l - \frac{\alpha}{2}) \tag{1}$$

In which α, P_u and P_l represents the volume fraction of porosities, the material properties of top and bottom sides, respectively. V_u and $V_l$are the volume fraction of top and bottom surfaces, respectively and are related by

$$V_u + V_l = 1 \tag{2}$$

Then the volume fraction of upper side (V_u) is defined as follows

$$V_u = (\frac{z}{h} + \frac{1}{2})^{P} \tag{3}$$

According to Eqs. (1)-(2), the effective material properties of porous MEE-FG(I) beam with even porosities are variable across the thickness direction with following form

$$P(z) = (P_u - P_l)\left(\frac{z}{h} + \frac{1}{2}\right)^{p} + P_l - (P_u + P_l)\frac{\alpha}{2} \tag{4}$$

The MEE-FG (II) beam has porosity phases spreading frequently nearby the middle zone of the cross-section and the amount of porosity seems to be linearly decrease to zero at the top and bottom of the cross-section. Fig. 1 demonstrates cross-section areas of FGM-I and-II with porosities phases. For uneven distribution of porosities, the effective material properties are replaced by following form.

$$\begin{aligned} P(z) = {} & (P_u - P_l)\left(\frac{z}{h} + \frac{1}{2}\right)^{p} \\ & + P_l - \frac{\alpha}{2}(P_u + P_l)(1 - \frac{2|z|}{h}) \end{aligned} \tag{5}$$

2.2 Kinematic relations

In view of new tangential-exponential refined shear deformation theory, the displacement field at any point of the beam can be expressed as

$$u_1(x,z,t) = u(x,t) - z\frac{\partial w_b}{\partial x} - f(z)\frac{\partial w_s}{\partial x} \tag{5}$$

$$u_3(x,z,t) = w_b(x,t) + w_s(x,t) \tag{6}$$

where u is displacement of mid-plane along x and w_b, w_s are the bending and shear components of transverse displacement of a point on the mid-plane of the beam. The shape function assessing the shear stress variation across the beam thickness is taken as $f(z)$. $f(z)$ is considered to satisfy the stress-free boundary conditions on the top and bottom sides of the beam. So, it is not required to use any shear correction factor. The present theory has a function in the form (Mantari *et al*. 2014)

$$f(z_{ns}) = tan\left[\left(\frac{\pi(z_{ns}+c)}{2h}\right)\right] r^{sec\left[\left(\frac{\pi(z_{ns}+c)}{2h}\right)\right]}, \quad r = 0.03 \tag{8}$$

The electric potential and magnetic potential distributions across the thickness are approximated via a combination of a cosine and linear variation to satisfy Maxwell's equation in the quasi-static approximation as follows (Ke and Wang 2014)

$$\Phi(x,z,t) = -cos(\xi(z))\phi(x,t) + \frac{2z}{h}V \tag{9}$$

$$\Upsilon(x,z,t) = -cos(\xi(z))\gamma(x,t) + \frac{2z}{h}\Omega \tag{10}$$

where $\xi = \pi/h$. V and Ω are the external electric voltage and magnetic potential applied to the MEE-FG beam. Nonzero strains of the four-variable beam model are written as

$$\varepsilon_x = \varepsilon_x^0 + z\kappa_x^b + f\kappa_x^s, \quad \gamma_{xz} = g\gamma_{xz}^s, g = 1 - \frac{\partial f}{\partial z} \tag{11}$$

where

$$\varepsilon_x^0 = \frac{\partial u}{\partial x}, \quad \kappa_x^b = -\frac{\partial^2 w_b}{\partial x^2}, \quad \kappa_x^s = -\frac{\partial^2 w_s}{\partial x^2}, \quad \gamma_{xz}^s = \frac{\partial w_s}{\partial x} \tag{12}$$

According to Eq. (9), the relation between electric field (E_x, E_y, E_z) and electric potential (Φ), can be obtained as

$$E_x = -\Phi_{,x} = cos(\xi z)\frac{\partial \phi}{\partial x}, \tag{13}$$

$$E_z = -\Phi_{,z} = -\xi\, sin(\xi(z))\phi - \frac{2V}{h} \tag{14}$$

Also, the relation between magnetic field (H_x, H_y, H_z) and magnetic potential (Υ) can be expressed from Eq. (10) as

$$H_x = -\Upsilon_{,x} = cos(\xi z)\frac{\partial \gamma}{\partial x}, \tag{15}$$

$$H_z = -\Upsilon_{,z} = -\xi\, sin(\xi z)\gamma - \frac{2\Omega}{h} \tag{16}$$

Through extended Hamilton's principle, the equation of motion can be viwed by

$$\int_0^t \delta(\Pi_S + \Pi_W)dt = 0 \tag{17}$$

where Π_S is strain energy, Π_W is work done by external forces. The following Euler–Lagrange equations are obtained by using the virtual work principle and setting the coefficients of $\delta u, \delta w_b, \delta w_s, \delta\phi$ and $\delta\gamma$ to zero

$$\frac{\partial N_x}{\partial x} = 0 \tag{18}$$

$$\frac{\partial^2 M_x^b}{\partial x^2} - \bar{N}\nabla^2(w_b + w_s) = 0 \tag{19}$$

$$\frac{\partial^2 M_x^s}{\partial x^2} + \frac{\partial Q_{xz}}{\partial x} - \bar{N}\nabla^2(w_b + w_s) = 0 \tag{20}$$

$$\int_{-h/2-C}^{h/2-C}\left(cos(\xi z)\frac{\partial D_x}{\partial x} + \xi\, sin(\xi z)D_z\right)dz = 0 \tag{21}$$

$$\int_{-h/2-C}^{h/2-C}\left(cos(\xi z)\frac{\partial B_x}{\partial x} + \xi\, sin(\xi z)B_z\right)dz = 0 \tag{22}$$

In which the variables introduced (N, M_b, M_s, Q), mass moment of inertias $(I_0, I_1, I_2, J_1, J_2, k_2)$ and in-plane applied load N_x^0 at the last expression are expressed by

$$(N, M_b, M_s) = \int_A \sigma_{xx}(1, z, f)\, dA, \quad (Q) = \int_A \sigma_{xz}(g)\, dA \tag{23}$$

For a linear MEE porous FG beam exposed to magneto-electro-thermo-mechanical loading, the coupled constitutive relations may be rewritten as

$$\sigma_{ij} = C_{ijkl}\varepsilon_{kl} - e_{mij}E_m - q_{nij}H_n \tag{24}$$

$$D_i = e_{ikl}\varepsilon_{kl} + k_{im}E_m + d_{in}H_n \tag{25}$$

$$B_i = q_{ikl}\varepsilon_{kl} + d_{im}E_m + \chi_{in}H_n \tag{26}$$

in which σ_{ij}, D_i, B_i explains the components of stress, electric displacement and magnetic induction, ε_{kl}, E_m and H_n are the components of linear strain, electric field and magnetic field. Further, C_{ijkl} , k_{im} and χ_{in} are the components of elastic stiffness, dielectric permittivity and magnetic permittivity coefficients; Finally, e_{mij}, q_{nij}, and d_{in} are the piezoelectric, piezo-magnetic, and magneto-electric-elastic coefficients, respectively. By integrating Eq. (24)-(26) over the area of MEE porous FG beam cross-section, the following relations for the force-strain and the moment-strain and other necessary relation of the refined FG beam can be obtained

$$N_x = A_{11}\frac{\partial u}{\partial x} - B_{11}\frac{\partial^2 w_b}{\partial x^2} - B_{11}^s\frac{\partial^2 w_s}{\partial x^2} + A_{31}^e\phi + A_{31}^m\gamma \tag{27}$$

$$M_x^b = B_{11}\frac{\partial u}{\partial x} - D_{11}\frac{\partial^2 w_b}{\partial x^2} - D_{11}^s\frac{\partial^2 w_s}{\partial x^2} + E_{31}^e\phi + E_{31}^m\gamma \tag{28}$$

$$M_x^s = B_{11}^s\frac{\partial u}{\partial x} - D_{11}^s\frac{\partial^2 w_b}{\partial x^2} - H_{11}^s\frac{\partial^2 w_s}{\partial x^2} + F_{31}^e\phi + F_{31}^m\gamma \tag{29}$$

$$Q_{xz} = A_{44}^s\frac{\partial w_s}{\partial x} - A_{15}^e\frac{\partial \phi}{\partial x} - A_{15}^m\frac{\partial \gamma}{\partial x} \tag{30}$$

$$\int_{-h/2-C}^{h/2-C} D_x\cos(\xi z)dz = E_{15}^{e}\frac{\partial w_s}{\partial x} + F_{11}^{e}\frac{\partial\phi}{\partial x} + F_{11}^{m}\frac{\partial\gamma}{\partial x} \quad (31)$$

$$\begin{aligned}&\int_{-\frac{h}{2}-C}^{\frac{h}{2}-C} D_z\xi\sin(\xi z)dz\\ &= A_{31}^{e}(\frac{\partial u}{\partial x}) - E_{31}^{e}\nabla^2 w_b - F_{31}^{e}\nabla^2 w_s - F_{33}^{e}\phi - F_{33}^{m}\gamma\end{aligned} \quad (32)$$

$$\begin{aligned}&\int_{-\frac{h}{2}-C}^{\frac{h}{2}-C} B_x\cos(\xi z)dz\\ &= E_{15}^{m}\frac{\partial w_s}{\partial x} + F_{11}^{m}\frac{\partial\phi}{\partial x} + X_{11}^{m}\frac{\partial\gamma}{\partial x}\end{aligned} \quad (33)$$

$$\begin{aligned}&\int_{-\frac{h}{2}-C}^{\frac{h}{2}-C} B_z\xi\sin(\xi z)dz\\ &= A_{31}^{m}(\frac{\partial u}{\partial x}) - E_{31}^{m}\nabla^2 w_b - F_{31}^{m}\nabla^2 w_s - F_{33}^{m}\phi - X_{33}^{m}\gamma\end{aligned} \quad (34)$$

in which the cross-sectional rigidities are defined as follows

$$\begin{aligned}&(A_{11}, B_{11}, B_{11}^{s}, D_{11}, D_{11}^{s}, H_{11}^{S})\\ &= \sum_{n=1}^{3}\int_{h_{n-1}}^{h_n} C_{11}(1, z, f, z^2, zf, f^2)\,dz, A_{44}^{s}\\ &= \sum_{n=1}^{3}\int_{h_{n-1}}^{h_n} c_{55}g^2 dz\end{aligned} \quad (35)$$

$$\begin{aligned}&\{A_{31}^{e}, E_{31}^{e}, F_{31}^{e}, A_{31}^{m}, E_{31}^{m}, F_{31}^{m}\}\\ &= \sum_{n=1}^{3}\int_{-h_{n-1}}^{h_n} \xi\sin(\xi z)\begin{Bmatrix} e_{31}, e_{31}z, e_{31}f, \\ q_{31}, q_{31}z, q_{31}f \end{Bmatrix} dz\end{aligned} \quad (36)$$

$$\begin{aligned}&\{A_{15}^{e}, E_{15}^{e}, A_{15}^{m}, E_{15}^{m}\}\\ &= \sum_{n=1}^{3}\int_{-h_{n-1}}^{h_n} \cos(\xi z)\{e_{15}, e_{15}g, q_{15}, q_{15}g\}\,dz\end{aligned} \quad (37)$$

$$\begin{aligned}&\{F_{11}^{e}, F_{33}^{e}, F_{11}^{m}, F_{33}^{m}\}\\ &= \sum_{n=1}^{3}\int_{-h_{n-1}}^{h_n} \begin{Bmatrix} k_{11}\cos^2(\xi z), k_{33}\xi^2\sin^2(\xi z), \\ d_{11}\cos^2(\xi z), d_{33}\xi^2\sin^2(\xi z) \end{Bmatrix} dz\end{aligned} \quad (38)$$

$$\begin{aligned}&\{X_{11}^{m}, X_{33}^{m}\}\\ &= \sum_{n=1}^{3}\int_{-h_{n-1}}^{h_n} \{\chi_{11}\cos^2(\xi z), \chi_{33}\xi^2\sin^2(\xi z)\}\,dz\end{aligned} \quad (39)$$

The displacement equation motion through refined four-variable shear deformation MEE porous FG beam can be derived by substituting Eqs. (27)-(34), into Eqs. (18)-(22) as follows

$$\begin{aligned}&A_{11}\frac{\partial^2 u}{\partial x^2} - B_{11}\frac{\partial^3 w_b}{\partial x^3} - B_{11}^{s}\frac{\partial^3 w_s}{\partial x^3}\\ &+A_{31}^{e}\frac{\partial\phi}{\partial x} + A_{31}^{m}\frac{\partial\gamma}{\partial x} = 0\end{aligned} \quad (40)$$

$$\begin{aligned}&B_{11}\frac{\partial^3 u}{\partial x^3} - D_{11}\frac{\partial^4 w_b}{\partial x^4} + E_{31}^{e}\frac{\partial^2\phi}{\partial x^2}\\ &-D_{11}^{s}\frac{\partial^4 w_s}{\partial x^4} + E_{31}^{m}\frac{\partial^2\gamma}{\partial x^2} - (\bar{N})\frac{\partial^2(w_b + w_s)}{\partial x^2} = 0\end{aligned} \quad (41)$$

$$\begin{aligned}&B_{11}^{s}\frac{\partial^3 u}{\partial x^3} - D_{11}^{s}\frac{\partial^4 w_b}{\partial x^4} + A_{55}^{s}\frac{\partial^2 w_s}{\partial x^2}\\ &-H_{11}^{s}\frac{\partial^4 w_s}{\partial x^4} + F_{31}^{e}\frac{\partial^2\phi}{\partial x^2} + F_{31}^{m}\frac{\partial^2\gamma}{\partial x^2}\\ &-(\bar{N})\frac{\partial^2(w_b + w_s)}{\partial x^2} - A_{15}^{e}\frac{\partial^2\phi}{\partial x^2} - A_{15}^{m}\frac{\partial^2\gamma}{\partial x^2} = 0\end{aligned} \quad (42)$$

$$\begin{aligned}&A_{31}^{e}\left(\frac{\partial u}{\partial x}\right) - E_{31}^{e}\frac{\partial^2 w_b}{\partial x^2} - F_{31}^{e}\frac{\partial^2 w_s}{\partial x^2} + E_{15}^{e}\frac{\partial^2 w_s}{\partial x^2}\\ &+F_{11}^{e}\frac{\partial^2\phi}{\partial x^2} + F_{11}^{m}\frac{\partial^2\gamma}{\partial x^2} - F_{33}^{e}\phi - F_{33}^{m}\gamma = 0\end{aligned} \quad (43)$$

$$\begin{aligned}&A_{31}^{m}\left(\frac{\partial u}{\partial x}\right) - E_{31}^{m}\frac{\partial^2 w_b}{\partial x^2} - F_{31}^{m}\frac{\partial^2 w_s}{\partial x^2} + E_{15}^{m}\frac{\partial^2 w_s}{\partial x^2}\\ &+F_{11}^{m}\frac{\partial^2\phi}{\partial x^2} + X_{11}^{m}\frac{\partial^2\gamma}{\partial x^2} - F_{33}^{m}\phi - X_{33}^{m}\gamma = 0\end{aligned} \quad (44)$$

In this study, it is assumed that the porous MEE-FG beam is under temperature rising and external electric voltage, magnetic potential and the shear loading is ignored. So $\bar{N}$ is the normal forces induced by temperature rising, external electric voltage V and external magnetic potential Ω, respectively and are defined as

$$\{N^E, N^H\} = -\int_{-h/2}^{h/2}\{\tilde{e}_{31}V, \tilde{q}_{31}\Omega\}\frac{2}{h}dz \quad (45)$$

$$N^T = \int_{-h/2}^{h/2} E(z)\alpha(z)\Delta T dz \quad (46)$$

$$\bar{N} = N^E + N^H + N^T \quad (47)$$

3. Thermal environment and temperature distributions

For a MEE porous FG beam in thermal environment, temperature is assumed vary along the thickness directions at three ways as:

3.1 Uniform temperature rise (UTR)

Consider a porous FG that is at reference temperature equal to $T_0 = 300$ and beam is free of stresses at T_0 and temperature of beam is uniformly raised to final temperature with the difference of ΔT as

$$\Delta T = T - T_0 \quad (48)$$

3.2 Linear temperature rise (LTR)

Consider the temperature of the top surface of the porous FG beam is T_t and vary linearly from T_t to T_b, the bottom surface temperature finally the temperature rise is given as (Kiani and Eslami 2013)

$$T = T_m + \Delta T\left(\frac{1}{2}+\frac{z}{h}\right) \tag{49}$$

$$\Delta T = T_t - T_b \tag{50}$$

3.3 Sinusoidal temperature rise (STR)

The temperature field when FG beam is exposed to sinusoidal temperature rise across the thickness can be defined as

$$T = T_m + \Delta T\left(1 - Cos\frac{\pi}{2}\left(\frac{1}{2}+\frac{z}{h}\right)\right) \tag{51}$$

where $\Delta T = T_c - T_m$ is temperature change.

4. Solution procedure

As given in Sobhy (2013), an exact solution of the governing equations for free vibration of a MEE porous FG beam with simply-supported (S), clamped (C) edges or combinations of these boundary conditions is presented as

Simply-supported (S): $w_b = w_s = N_x = M_x = 0$ at $x = 0, L$ (52)

Clamped (C): $u = w_b = w_s = \frac{\partial w_b}{\partial x} = \frac{\partial w_s}{\partial x} = 0$ at $x = 0, L$ (53)

To satisfy above-mentioned boundary conditions, the displacement quantities are presented in the following form

$$U = \sum_{m=1}^{\infty} U_m \frac{\partial X_m(x)}{\partial x} e^{iw_m t} \tag{54}$$

$$\{W_b, W_s, \phi, \gamma\} = \sum_{m=1}^{\infty}\{W_{bm}, W_{sm}, \Phi_m, Y_m\}X_m(x)\, e^{iw_m t} \tag{55}$$

where (U_{mn}, W_{bmn}, W_{smn}, Φ_{mn}, γ_{mn}) are the unknown coefficients and the function $X_m$and are tabulated in detail in Table 2 for different boundary conditions ($\alpha = m\pi/a$, $\beta = n\pi/b$). Inserting Eqs. (66)-(70) into Eqs. (54)-(58) respectively, leads to

$$\begin{gathered}[A_{11}r_3]U_m - [B_{11}r_3]W_b - [B_{11}^s r_3]W_s \\ +[A_{31}^e r_1]\Phi_m + [A_{31}^m r_1]Y_m = 0\end{gathered} \tag{56}$$

$$\begin{gathered}[B_{11}r_9]U_m - \left[D_{11}r_9 + \bar{N}r_{7_5}\right]W_{bm} \\ -[D_{11}^s r_9 + \bar{N}r_7]W_{sm} + [E_{31}^e r_7]\Phi_m + [E_{31}^m r_7]Y_m = 0\end{gathered} \tag{57}$$

$$\begin{gathered}[B_{11}^s r_9]U_m + \left[-D_{11}^s r_{9_5} - \bar{N}r_7\right]W_{bm} \\ +[-H_{11}^s r_9 + (A_{55}^s - \bar{N})r_7]W_{sm} \\ +[(F_{31}^e - A_{15}^e)r_7]\Phi_m + ([F_{31}^m - A_{15}^m)r_7]Y_m = 0\end{gathered} \tag{58}$$

Table 2 The admissible functions $X_m(x)$ (Sobhy 2013)

	Boundary conditions	The functions $\boldsymbol{X_m}$
	At $x = 0,\ a$	$X_m(x)$
SS	$x_m(0) = x_m''(0) = x_m(a) = x_m''(a) = 0$	$Sin(\alpha x)$
CS	$x_m(0) = x_m'(0) = x_m(a) = x_m''(a) = 0$	$Sin(\alpha x)[Cos(\alpha x) - 1]$
CC	$x_m(0) = x_m'(0) = x_m(a) = x_m'(a) = 0$	$\mathrm{Sin}^2(\alpha x)$

$$\begin{gathered}A_{31}^e r_7 U_m - E_{31}^e r_7 W_{bm} + (E_{15}^e - F_{31}^e)r_7 W_{sm} \\ +(F_{11}^e r_7 - F_{33}^e r_5)\Phi_m + (F_{11}^m r_7 - F_{33}^m r_5)Y_m = 0\end{gathered} \tag{59}$$

$$\begin{gathered}A_{31}^m r_7 U_m - E_{31}^m r_7 W_{bm} + (E_{15}^m - F_{31}^m)r_7 W_{sm} \\ +(F_{11}^m r_7 - F_{33}^m r_5)\Phi_m + [X_{11}^m r_7 - X_{33}^m r_5]Y_m = 0\end{gathered} \tag{60}$$

where

$$(r_3, r_1) = \int_0^L \left(\frac{\partial^3 X_m}{\partial x^3}, \frac{\partial X_m}{\partial x}\right)\frac{\partial X_m}{\partial x} \tag{61}$$

$$(r_5, r_7, r_9) = \int_0^L \left(X_m, \frac{\partial^2 X_m}{\partial x^2}, \frac{\partial^4 X_m}{\partial x^4}\right)X_m \tag{62}$$

By finding determinant of the coefficient matrix of the following equations and setting this multinomial to zero, we can find critical buckling temperature ΔT_{cr}.

$$\begin{bmatrix} k_{11} & k_{12} & k_{13} & k_{14} & k_{15} \\ k_{21} & k_{22} & k_{23} & k_{24} & k_{25} \\ k_{31} & k_{32} & k_{33} & k_{34} & k_{35} \\ k_{41} & k_{42} & k_{43} & k_{44} & k_{45} \\ k_{51} & k_{52} & k_{53} & k_{54} & k_{55} \end{bmatrix}\begin{bmatrix} U_{mn} \\ W_{bmn} \\ W_{smn} \\ \psi_{mn} \\ \gamma_{mn} \end{bmatrix} = 0 \tag{63}$$

5. Numerical results and discussions

In this section, numerical and graphical examples are presented to examine magneto-electro-thermo-mechanical buckling behavior of MEE-FG beam subjected to various thermal loadings with porosities employing a higher order refined beam theory. So, the influences of temperature rising, porosity volume fraction, FG material graduation, magnetic and electric fields, different types of porosity distributions and various boundary conditions on the critical buckling temperatures of the MEE porous FG beam will be provided as dispersion curves. It evident that the present beam model and solution procedure can accurately predict buckling loads of FGM beam. For comparison study, the material properties are selected as: E_c = 380 GPa, E_m = 70 GPa and $\nu = 0.3$ .The non-dimensional buckling load ($\bar{N}_{cr}$) can be calculated by the relation in Eq. (64) as

$$\overline{N}_{cr} = \overline{N}\frac{L^2}{c_{11}^u I} \tag{64}$$

In Table 4, the effect of porosity volume fraction, temperature rising and electric voltage on the critical

Table 3 Comparison of non-dimensional buckling load of FGM beam for various power-law exponents

L/h		p = 0	p = 0.5	p = 1	p = 2	p = 5	p = 10
5		48.8406	32.0013	24.6894	19.1577	15.7355	14.1448
	Present	48.835	31.967	24.6870	19.1605	15.7401	14.13
10		52.3083	34.0002	26.1707	20.3909	17.1091	15.5278
	Present	52.3082	34.0087	26.1727	20.3936	17.1118	15.5291

Table 4 The variation of the critical buckling temperature (ΔT_{cr}) of MEE FG beam subjected to different temperature loadings for various external electric voltage and boundary conditions $(L/h = 20,\ \Omega = 0,\ p = 1)$

Type of FG		S-S			C-S			C-C		
		V = -250	V = 0	V = +250	V = -250	V = 0	V = +250	V = -250	V = 0	V = +250
UTR	Perfect	30.4372	30.0508	29.6645	74.3944	74.008	73.6217	117.263	116.876	116.49
	α = 0.2, even	35.7459	35.2575	34.769	87.213	86.7246	86.2361	137.3	136.811	136.323
	α = 0.2, uneven	35.5979	35.1684	34.7389	87.0365	86.607	86.1775	137.197	136.767	136.338
LTR	Perfect	50.1296	49.3682	48.6068	136.757	135.996	135.234	221.239	220.477	219.716
	α = 0.2, even	60.3581	59.3992	58.4403	161.395	160.436	159.477	259.721	258.762	257.803
	α = 0.2, uneven	60.1473	59.303	58.4587	161.262	160.417	159.573	259.864	259.019	258.175
STR	Perfect	68.7455	67.7014	66.6572	187.542	186.498	185.454	303.397	302.353	301.309
	α = 0.2, even	82.7789	81.4638	80.1488	221.347	220.032	218.717	356.198	354.883	353.567
	α = 0.2, uneven	80.7211	79.588	78.4549	216.422	215.289	214.156	348.752	347.619	346.486

Table 5 The variation of the critical buckling temperature (ΔT_{cr}) of MEE FG beam subjected to different temperature loadings for various magnetic potential and boundary conditions $(L/h = 20,\ \Omega = 0,\ p = 1)$

Type of FG		S-S			C-S			C-C		
		Ω = -25	Ω = 0	Ω = +25	Ω = -25	Ω = 0	Ω = +25	Ω = -25	Ω = 0	Ω = +25
UTR	Perfect	24.9553	30.0508	35.1464	68.9125	74.008	79.1035	111.781	116.876	121.972
	α = 0.2, even	28.8155	35.2575	41.6994	80.2826	86.7246	93.1665	130.369	136.811	143.253
	α = 0.2, uneven	29.5039	35.1684	40.833	80.9424	86.607	92.2715	131.103	136.767	142.432
LTR	Perfect	39.3263	49.3682	59.4101	125.954	135.996	146.037	210.435	220.477	230.519
	α = 0.2, even	46.7528	59.3992	72.0456	147.789	160.436	173.082	246.116	258.762	271.408
	α = 0.2, uneven	48.168	59.303	70.4379	149.282	160.417	171.552	247.884	259.019	270.154
STR	Perfect	53.9304	67.7014	81.4723	172.727	186.498	200.269	288.582	302.353	316.124
	α = 0.2, even	64.1198	81.4638	98.8079	202.688	220.032	237.376	337.538	354.883	372.227
	α = 0.2, uneven	64.6443	79.588	94.5317	200.345	215.289	230.233	332.675	347.619	362.562

buckling temperature of the MEE-porous FG beam are listed for various boundary conditions (S-S, C-S, C-C), different porosity parameters($\alpha = 0,\ 0.2$), external electric voltage (V = -250, 0, 250) and two porosity distributions (even, uneven) at Ω = 0, p = 1. Also, Table 5 present the critical buckling temperature of smart FG porous beam for different boundary conditions (S-S, C-S, C-C), magnetic potentials (-25, 0, 25), porosity volume fraction (α = 0, α = 0.2) and two porosity distributions (even, uneven) at V = 0 and p=1. From the results of these tables, it is found that the porosity leads substantial growth on the critical buckling temperature of MEE-FG (I) & (II) beam for all of the boundary conditions and thermal loadings. It is seen that external electric voltage and magnetic field has an important role on the buckling behavior of the structure, where the effect of them depends on the sign of electric voltage and magnetic potential, in other words negative values of electric voltage leads to increase the critical buckling temperature of the smart FG porous beam while, positive values of electric voltage have reverse trend. On the opposite side, magnetic field has an opposite behavior. This means that negative and positive values of magnetic field are cause of tensile and compressive of critical buckling temperature, respectively. Comparing the critical buckling temperature of smart FG beam for different boundary conditions expresses that the greatest critical buckling temperature is obtained for MEE-porous FG beam with C-C boundary condition followed with other boundary

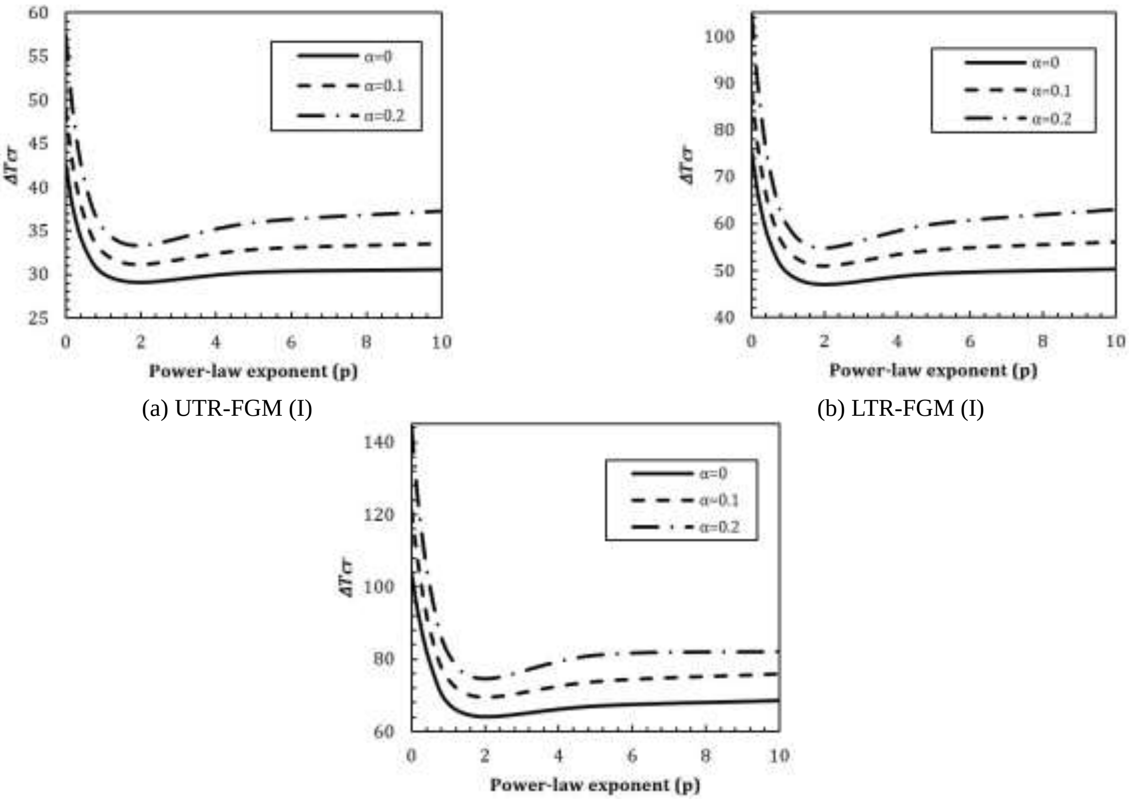

(a) UTR-FGM (I)

(b) LTR-FGM (I)

(c) STR-FGM (I)

Fig. 2 The variation of the critical buckling temperature of S-S MEE-FG (I) & (II) beam with respect to material graduation and porosity parameter for different temperature risings $(\Omega = 0,\ V = 0)$

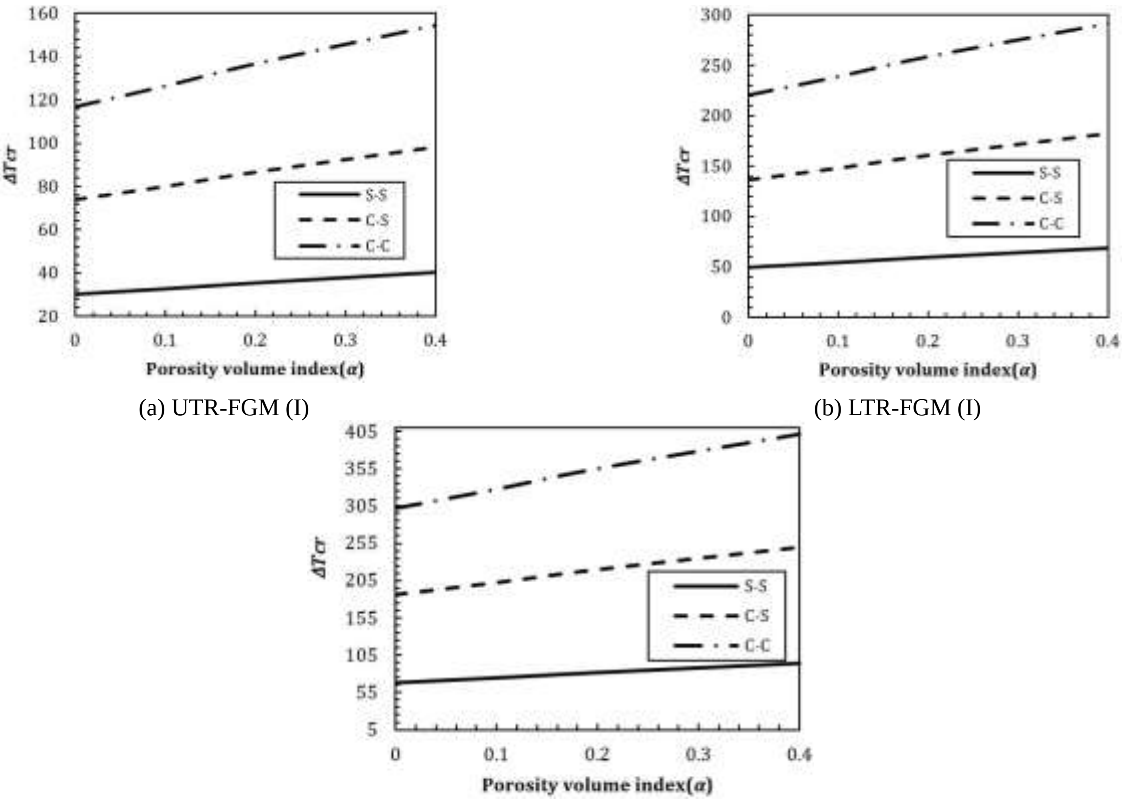

(a) UTR-FGM (I)

(b) LTR-FGM (I)

(c) STR-FGM (I)

Fig. 3 The effect of porosity volume index on the critical buckling temperature of MEE-FG (I) & (II) beam with respect to temperature rising and for different boundary conditions $(p = 1,\ \Omega = 0,\ V = 0)$

conditions. Comparing results of different temperature field reveals that sinusoidal temperature rising (STR) provide highest critical buckling temperature and UTR present lowest temperature.

In order to peruse the effect of the porosity volume fraction and thermal loading type on the critical buckling temperatures of the smart SS MEE porous FG (I) beam, critical buckling temperatures (ΔT_{cr}), versus the power-law index (p) for different volume fractions of porosity (α = 0, 0.1, 0.2) magnetic potential (Ω = 0) and electric voltage (V = 0) is plotted in Fig. 2. From the dispersion curves, it is seen that growing of the power-law exponents is cause of reduction in the critical buckling temperatures of both porosity distributions. As one can see, the critical buckling temperatures decreases more intensity where the material graduation is in range from 0 to 2 than that where the material graduation is in range between 2 and 10. In fact, when p = 0 beam is made from fully $\mathrm{CoFe_2}O_4$ and has the greatest critical buckling temperatures. Increasing the material graduation exponent from 0 to 10 changes the composition of the MEE-FG beam from a fully $\mathrm{CoFe_2}O_4$ beam to a beam with a combination of $\mathrm{CoFe_2}O_4$ and $\mathrm{BaTio_3}$. So, by increasing the metal percentage and having the lower value of Young's modulus of $\mathrm{BaTio_3}$ with respect to $\mathrm{CoFe_2}O_4$, the stiffness of system diminishes. Thus, critical buckling temperatures decay as the stiffness of a structure decreasing. Moreover, it is found that the porosity effect on the buckling behavior of smart FG beam is as follow: The critical buckling temperatures grow as the porosity parameter (α) increases for each of power-law

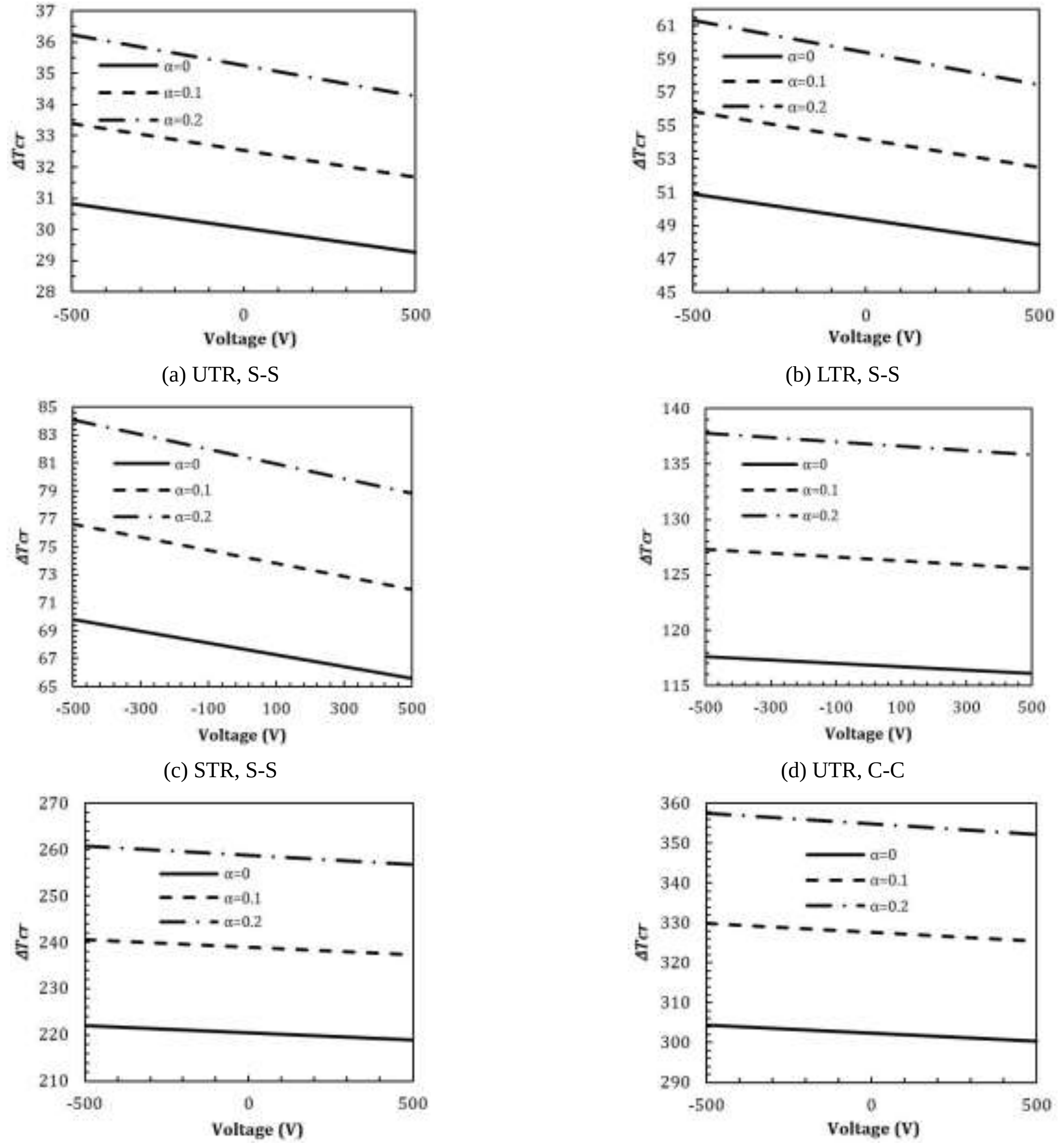

(a) UTR, S-S

(b) LTR, S-S

(c) STR, S-S

(d) UTR, C-C

(e) LTR, C-C

(f) STR, C-C

Fig. 4 The influence of electric voltage and porosity parameter on the critical buckling temperature of MEE-FG (I) beam subjected to different temperature rising (UTR, LTR, STR) &($p = 1,\ \Omega = 0$)

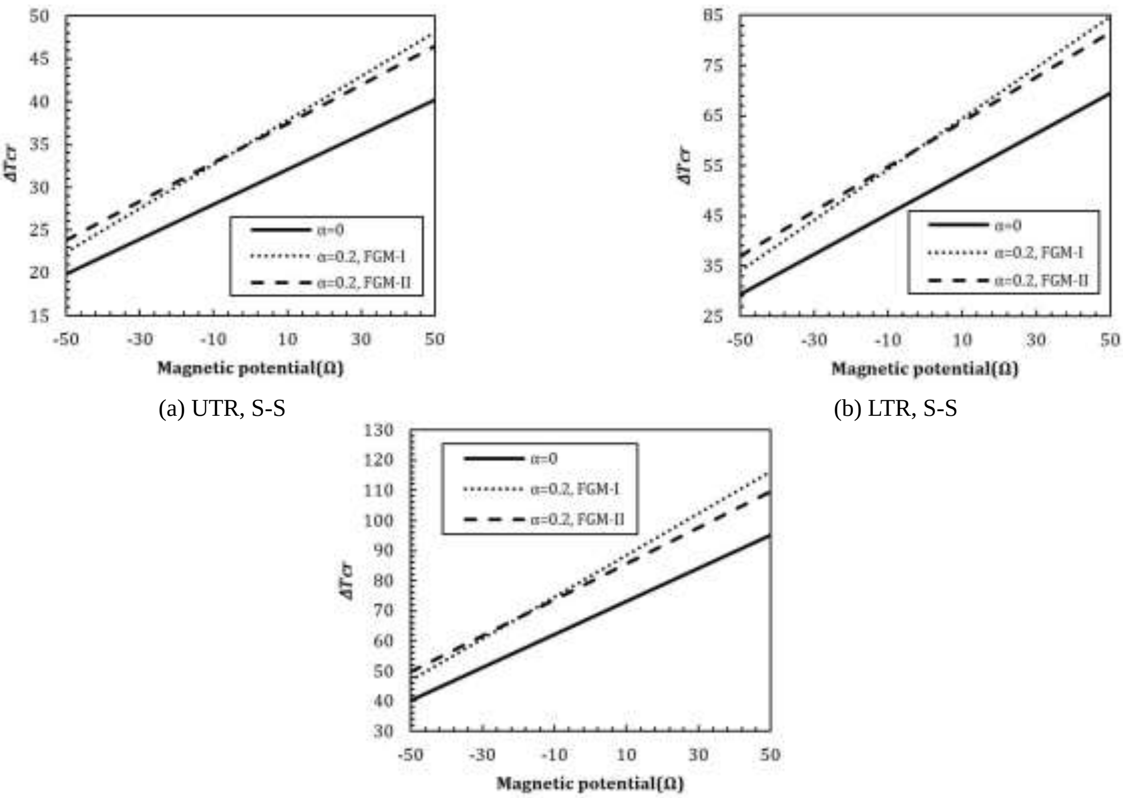

(a) UTR, S-S

(b) LTR, S-S

(c) STR, S-S

Fig. 5 The influence of magnetic potential on the critical buckling temperature of MEE perfect and imperfect FG beam subjected to different temperature rising (UTR, LTR, STR) &$(p = 1,\ V = 0)$

index values. So, it is clear that the porosity effect becomes outstanding for MEE-FG beam. Comparing the results of different temperature risings divulges the critical buckling temperature of MEE-FG beam exposed to sinusoidal temperature rise (STR) is highest temperature. Whereas UTR provide the lower values of critical buckling temperature. To display the influence of boundary conditions on the critical buckling temperature of MEE-FG (I) & (II) beam for different temperature field (UTR, LTR, STR), Fig. 3 demonstrates the critical buckling temperature results versus porosity parameters via three boundary conditions (SS, CS, CC) at constant value of power-law index (p = 1) electric voltage (V = 0) and magnetic potential $(\Omega = 0)$. As can be seen, increment of porosity parameter leads to increasing of critical buckling temperature of MEE-FG for all of the boundary conditions. Here, the critical buckling temperature of porous MEE-FGM beam with CC boundary conditions is greatest, followed by CS and SS respectively. The impact of electric voltage on the critical buckling temperature of smart MEE-FG (I) beam subjected to different temperature fields (UTR, LTR, STR) with S-S and C-C boundary conditions is illustrated in Fig. 4, respectively. The porosity volume fractions (α = 0, 0.1, 0.2) at $\Omega = 0$ and p = 1 is taken. It is obvious that when the intensity of external electric voltage increases from negative to positive value, the critical buckling temperature of MEE-FG porous beam reduce for all of the thermal loadings. Also, it is observed that the impact of the external electric voltage on the critical buckling temperature of S-S MEE-FG beam is more eminent than that of the C-C MEE-FG beam. So, it is very momentous to attention the type of boundary conditions of MEE-FG porous beam. Also, the greatest buckling temperature of MEE-FG beam is obtained for the beam subjected to STR temperature rising followed by LTR and UTR respectively. Fig. 5 discuss the variations of critical buckling temperature of S-S MEE-FG porous beam versus magnetic potential via different thermal loadings (UTR, LTR, STR) for perfect and imperfect FGM (even and uneven) at p = 1, V = 0. It is pointed that increasing of the external magnetic potential is cause of increment in critical buckling temperature when their values vary from negative to positive one at a fixed value of porosity volume fraction which highlights the notability of the magnitude and sign of magnetic potential. So, it is very important to regard the magnetic field in the analysis of MEE-FG beam with porosity. Furthermore, according to these results the critical buckling temperature increases as the porosity value increases for all values of magnetic potential. By comparing the porosity distributions, it is concluded that at first MEE-FG beam with uneven porosity presents higher critical buckling temperature. Then, with the increasing of external magnetic potential, it is seen that MEE-FG with even porosity provided higher temperature.

6. Conclusions

Based on four-variable higher order shear deformation beam theory, an analytical method solution is developed for buckling behavior of porous magneto-electro-elastic functionally graded beam in the view of different thermal loadings via different boundary conditions. Refined shear deformation theory predicts shear deformation effect without any shear correction factors. Two model of porosity distributions, namely even and uneven are considered. Magneto-electro-thermo-mechanical characteristics of the smart porous MEE-FG beam are gradually grow in the thickness direction via modified rule of mixture. The equations of motion and boundary conditions are derived by using Hamilton principle. An analytical solution method is used to solve governing partial differential equations for various boundary conditions. It is observed from the result that the critical buckling temperature of porous MEE-FGM beam are affected by thermal loading, magnetic field, external electric voltage, volume fraction of porosity, material graduation, various boundary conditions and porosity distributions. Numerical results show that:

- ✓ By increasing the material graduation index value, the critical buckling temperature of porous MEE-FG beam are found to decrease.
- ✓ For MEE-FGM beam with porosities, increasing the volume fraction of porosity yields increment in critical buckling temperature for both types of porosity distribution.
- ✓ Increasing magnetic potential from negative to positive values yields increment of critical buckling temperature of porous MEE-FGM beam. However, for the external electric voltage this behavior is opposite.
- ✓ The critical buckling temperature of porous MEE-FGM beam with C-C boundary conditions is greatest, followed by C-S and S-S.
- ✓ MEE-FG porous beam subjected to sinusoidal temperature rising (STR) provide highest critical buckling temperature and UTR present lowest temperature.

References

Atmane, H.A., Tounsi, A. and Bernard, F. (2015), "Effect of thickness stretching and porosity on mechanical response of a functionally graded beams resting on elastic foundations", *Int. J. Mech. Mater. Des.*, **13**(1), 71-84. https://doi.org/10.1007/s10999-015-9318-x

Barati, M.R., Zenkour, A.M. and Shahverdi, H. (2016), "Thermo-mechanical buckling analysis of embedded nanosize FG plates in thermal environments via an inverse cotangential theory", *Compos. Struct.*, **141**, 203-212. https://doi.org/10.1016/j.compstruct.2016.01.056

Boutahar, L. and Benamar, R. (2016), "A homogenization procedure for geometrically non-linear free vibration analysis of functionally graded annular plates with porosities, resting on elastic foundations", *Ain Shams Eng. J.*, **7**(1), 313-333. https://doi.org/10.1016/j.asej.2015.11.016

Ebrahimi, F. and Barati, M.R. (2016a), "A nonlocal higher-order refined magneto-electro-viscoelastic beam model for dynamic analysis of smart nanostructures", *Int. J. Eng. Sci.*, **107**, 183-196. https://doi.org/10.1016/j.ijengsci.2016.08.001

Ebrahimi, F. and Barati, M.R. (2016b), "Vibration analysis of nonlocal beams made of functionally graded material in thermal environment", *Eur. Phys. J. Plus*, **131**(8), 279. https://doi.org/10.1140/epjp/i2016-16279-y

Ebrahimi, F. and Hashemi, M. (2015), "On vibration behavior of rotating functionally graded double-tapered beam with the effect of porosities", *Proceedings of the Institution of Mechanical Engineers, Part G: J. Aerosp. Eng.*, 0954410015619647. https://doi.org/10.1177/0954410015619647

Ebrahimi, F. and Jafari, A. (2016a), "A higher-order thermomechanical vibration analysis of temperature-dependent FGM beams with porosities", *J. Eng.*, **2016**, 9561504. https://doi.org/10.1155/2016/9561504

Ebrahimi, F. and Jafari, A. (2016b), "Thermo-mechanical vibration analysis of temperature-dependent porous FG beams based on Timoshenko beam theory", *Struct. Eng. Mech., Int. J.*, **59**(2), 343-371. https://doi.org/10.12989/sem.2016.59.2.343

Ebrahimi, F. and Mokhtari, M. (2015), "Transverse vibration analysis of rotating porous beam with functionally graded microstructure using the differential transform method", *J. Brazil. Soc. Mech. Sci. Eng.*, **37**(4), 1435-1444. https://doi.org/10.1007/s40430-014-0255-7

Ebrahimi, F. and Zia, M. (2015), "Large amplitude nonlinear vibration analysis of functionally graded Timoshenko beams with porosities", *Acta Astronautica*, **116**, 117-125. https://doi.org/10.1016/j.actaastro.2015.06.014

Ebrahimi, F., Ghasemi, F. and Salari, E. (2016), "Investigating thermal effects on vibration behavior of temperature-dependent compositionally graded Euler beams with porosities", *Meccanica*, **51**(1), 223-249. https://doi.org/10.1007/s11012-015-0208-y

Henderson, J.P., Plummer, A. and Johnston, N. (2018), "An electro-hydrostatic actuator for hybrid active-passive vibration isolation", *Int. J. Hydromechatron.*, **1**(1), 47-71.

Jiang, A. and Ding, H. (2004), "Analytical solutions to magneto-electro-elastic beams", *Struct. Eng. Mech., Int. J.*, **18**(2), 195-209. https://doi.org/10.12989/sem.2004.18.2.195

Kadoli, R., Akhtar, K. and Ganesan, N. (2008), "Static analysis of functionally graded beams using higher order shear deformation theory", *Appl. Mathe. Model.*, **32**(12), 2509-2525. https://doi.org/10.1016/j.apm.2007.09.015

Kant, T. and Swaminathan, K. (2000), "Analytical solutions using a higher order refined theory for the stability analysis of laminated composite and sandwich plates", *Struct. Eng. Mech., Int. J.*, **10**(4), 337-357. https://doi.org/10.12989/sem.2000.10.4.337

Kattimani, S. and Ray, M. (2015), "Control of geometrically nonlinear vibrations of functionally graded magneto-electro-elastic plates", *Int. J. Mech. Sci.*, **99**, 154-167. https://doi.org/10.1016/j.ijmecsci.2015.05.012

Ke, L.-L. and Wang, Y.-S. (2014), "Free vibration of size-dependent magneto-electro-elastic nanobeams based on the nonlocal theory", *Physica E: Low-dimens. Syst. Nanostruct.*, **63**, 52-61. https://doi.org/10.1016/j.physe.2014.05.002

Ke, L.-L., Yang, J., Kitipornchai, S. and Bradford, M.A. (2012), "Bending, buckling and vibration of size-dependent functionally graded annular microplates", *Compos. Struct.*, **94**(11), 3250-3257. https://doi.org/10.1016/j.compstruct.2012.04.037

Khor, K. and Gu, Y. (2000), "Effects of residual stress on the performance of plasma sprayed functionally graded ZrO_2/NiCoCrAlY coatings", *Mater. Sci. Eng.: A*, **277**(1), 64-76. https://doi.org/10.1016/S0921-5093(99)00565-1

Kiani, Y. and Eslami, M. (2013), "An exact solution for thermal buckling of annular FGM plates on an elastic medium", *Compos. Part B: Eng.*, **45**(1), 101-110. https://doi.org/10.1016/j.compositesb.2012.09.034

Larbi, L.O., Kaci, A., Houari, M.S.A. and Tounsi, A. (2013), "An

Efficient Shear Deformation Beam Theory Based on Neutral Surface Position for Bending and Free Vibration of Functionally Graded Beams#", *Mech. Based Des. Struct. Mach.*, **41**(4), 421-433. https://doi.org/10.1080/15397734.2013.763713

Liew, K., Yang, J. and Kitipornchai, S. (2004), "Thermal post-buckling of laminated plates comprising functionally graded materials with temperature-dependent properties", *J. Appl. Mech.*, **71**(6), 839-850. https://doi.org/10.1115/1.1795220

Lu, C.-F. and Chen, W. (2005), "Free vibration of orthotropic functionally graded beams with various end conditions", *Struct. Eng. Mech., Int. J.*, **20**(4), 465-476. https://doi.org/10.12989/sem.2005.20.4.465

Mantari, J., Bonilla, E. and Soares, C.G. (2014), "A new tangential-exponential higher order shear deformation theory for advanced composite plates", *Compos. Part B: Eng.*, **60**, 319-328. https://doi.org/10.1016/j.compositesb.2013.12.001

Mechab, I., Mechab, B., Benaissa, S., Serier, B. and Bouiadjra, B.B. (2016), "Free vibration analysis of FGM nanoplate with porosities resting on Winkler Pasternak elastic foundations based on two-variable refined plate theories", *J. Brazil. Soc. Mech. Sci. Eng.*, **38**(8), 2193-2211. https://doi.org/10.1007/s40430-015-0482-6

Peng, X., Yan, M. and Shi, W. (2007), "A new approach for the preparation of functionally graded materials via slip casting in a gradient magnetic field", *Scripta Materialia*, **56**(10), 907-909. https://doi.org/10.1016/j.scriptamat.2006.12.020

Rezaei, A. and Saidi, A. (2016), "Application of Carrera Unified Formulation to study the effect of porosity on natural frequencies of thick porous–cellular plates", *Compos. Part B: Eng.*, **91**, 361-370. https://doi.org/10.1016/j.compositesb.2015.12.050

Seifried, S., Winterer, M. and Hahn, H. (2001), "Nanocrystalline gradient films through chemical vapor synthesis", *Scripta Materialia*, **44**(8), 2165-2168. https://doi.org/10.1016/S1359-6462(01)00898-3

Şimşek, M. and Yurtcu, H. (2013), "Analytical solutions for bending and buckling of functionally graded nanobeams based on the nonlocal Timoshenko beam theory", *Compos. Struct.*, **97**, 378-386. https://doi.org/10.1016/j.compstruct.2012.10.038

Sladek, J., Sladek, V., Krahulec, S., Chen, C. and Young, D. (2015), "Analyses of circular magnetoelectroelastic plates with functionally graded material properties", *Mech. Adv. Mater. Struct.*, **22**(6), 479-489. https://doi.org/10.1080/15376494.2013.807448

Sobhy, M. (2013), "Buckling and free vibration of exponentially graded sandwich plates resting on elastic foundations under various boundary conditions", *Compos. Struct.*, **99**, 76-87. https://doi.org/10.1016/j.compstruct.2012.11.018

Song, C., Xu, Z. and Li, J. (2007), "Structure of in situ Al/Si functionally graded materials by electromagnetic separation method", *Mater. Des.*, **28**(3), 1012-1015. https://doi.org/10.1016/j.matdes.2005.11.007

Tahouneh, V. (2014), "Free vibration analysis of bidirectional functionally graded annular plates resting on elastic foundations using differential quadrature method", *Struct. Eng. Mech., Int. J.*, **52**(4), 663-686. https://doi.org/10.12989/sem.2014.52.4.663

Tanaka, Y. (2018), "Active vibration compensator on moving vessel by hydraulic parallel mechanism", *Int. J. Hydromechatron.*, **1**(3), 350-359. https://doi.org/10.1504/IJHM.2018.094887

Vo, T.P., Thai, H.-T., Nguyen, T.-K. and Inam, F. (2014), "Static and vibration analysis of functionally graded beams using refined shear deformation theory", *Meccanica*, **49**(1), 155-168. https://doi.org/10.1007/s11012-013-9780-1

Vo, T.P., Thai, H.-T., Nguyen, T.-K., Inam, F. and Lee, J. (2015), "A quasi-3D theory for vibration and buckling of functionally graded sandwich beams", *Compos. Struct.*, **119**, 1-12. https://doi.org/10.1016/j.compstruct.2014.08.006

Wang, Z., Xie, Z. and Huang, W. (2018), "A pin-moment model of flexoelectric actuators", *Int. J. Hydromechatron.*, **1**(1), 72-90.

Watanabe, Y., Eryu, H. and Matsuura, K. (2001), "Evaluation of three-dimensional orientation of Al_3Ti platelet in Al-based functionally graded materials fabricated by a centrifugal casting technique", *Acta Materialia*, **49**(5), 775-783. https://doi.org/10.1016/S1359-6454(00)00384-0

Wattanasakulpong, N. and Ungbhakorn, V. (2014), "Linear and nonlinear vibration analysis of elastically restrained ends FGM beams with porosities", *Aerosp. Sci. Technol.*, **32**(1), 111-120. https://doi.org/10.1016/j.ast.2013.12.002

Wattanasakulpong, N., Prusty, B.G., Kelly, D.W. and Hoffman, M. (2012), "Free vibration analysis of layered functionally graded beams with experimental validation", *Mater. Des.*, **36**, 182-190. https://doi.org/10.1016/j.matdes.2011.10.049

Xin, L. and Hu, Z. (2015), "Free vibration of layered magneto-electro-elastic beams by SS-DSC approach", *Compos. Struct.*, **125**, 96-103. https://doi.org/10.1016/j.compstruct.2015.01.048

Yahia, S.A., Atmane, H.A., Houari, M.S.A. and Tounsi, A. (2015), "Wave propagation in functionally graded plates with porosities using various higher-order shear deformation plate theories", *Struct. Eng. Mech., Int. J.*, **53**(6), 1143-1165. https://doi.org/10.12989/sem.2015.53.6.1143

Yang, J., Liew, K. and Kitipornchai, S. (2006), "Imperfection sensitivity of the post-buckling behavior of higher-order shear deformable functionally graded plates", *Int. J. Solids Struct.*, **43**(17), 5247-5266. https://doi.org/10.1016/j.ijsolstr.2005.06.061

Zhu, J., Lai, Z., Yin, Z., Jeon, J. and Lee, S. (2001), "Fabrication of ZrO_2–NiCr functionally graded material by powder metallurgy", *Mater. Chem. Phys.*, **68**(1), 130-135. https://doi.org/10.1016/S0254-0584(00)00355-2

CC